Low-noise large-bandwidth high-gain transimpedance amplifier for cryogenic STM at 77 K

Ying-Xin Liang[1]*, Ru-Nan Shang[1], Fang-Hao Liang[2], Hao Zhang[1,3], Ke He[1,3,4]
[1]Beijing Academy of Quantum Information Sciences,Haidian, 100193, beijing, China
[2]School of Mathematics, Shandong University, Jinan 250100, Shandong, China
[3]State Key Laboratory of Low Dimensional Quantum Physics,
Department of Physics, Tsinghua University, Haidian, 100084, beijing, China
[4]Hefei National Laboratory, Hefei 230088, China

May 1, 2024

Abstract

In this work, we design and fabricate the transimpedance Amplifier (TIA) following the design mentioned in Ref.[1]. In the TIA, the preamplifier (Pre-Amp) is made of a junction field effect transistor (JFET) that can work at 77 K. The post-amplifier (Post-Amp) is made of an operational amplifier. Cascade Pre-Amp and Post-Amp to form the inverting-amplifier. With a 1.13 GΩ feedback network, the gain of TIA is 1.13 GΩ and its bandwidth is about 97 kHz. The equivalent input noise voltage power spectral density of TIA is not more than 9 $(\mathrm{nV})^2/\mathrm{Hz}$ at 10 kHz and 4 $(\mathrm{nV})^2/\mathrm{Hz}$ at 50kHz, and its equivalent input noise current power spectral density is about 26 $(\mathrm{fA})^2/\mathrm{Hz}$ at 10 kHz and 240 $(\mathrm{fA})^2/\mathrm{Hz}$ at 50 kHz. The measured transport performances and noise performances of TIA are consistent with the simulations and calculations. As an example, the realization of TIA in this work verifies the design method and analytical calculations for the low-noise large-bandwidth high-gain TIA proposed in Ref.[1, 2]. And, the TIA in this work is perfect for the cryogenic STM working at liquid nitrogen temperature.

1 Introduction

For cryogenic scanning tunneling microscope (CryoSTM), scanning tunneling spectroscopy (STS) and scanning tunnel shot noise spectroscopy (STSNS) [1, 2] are important means to investigate novel phenomena in quantum systems. High performance transimpedance amplifier (TIA) is a key element in CryoSTM for STS and STSNS measurements. The gain and bandwidth of TIA, as well as its inherent noise, determine its performance in the measurements. For a TIA, the inherent noise is characterized by equivalent input noise voltage and equivalent input noise current. And, the noise parameters are typically equivalent input noise voltage power spectral density (PSD) and equivalent input noise current PSD. Commercial TIAs for CryoSTM, such as FEMTO DE-DLPC-200 [3], as its gain is 1 GΩ, its bandwidth is only 1 kHz, and its equivalent input noise voltage PSD

*cryoliang@qq.com

is 16 $(\text{nV})^2/$ Hz in the frequencies of $f > 100$ Hz, and its equivalent input noise current PSD is 18.5 $(\text{fA})^2/$ Hz at $f = 100$ Hz. In recent years, several designs of TIA in CryoSTM are proposed based on new design ideas [1, 2, 4]. For them, the pre-amplifier are made of the low noise cryogenic HEMTs that are developed by CNRS/LPN France, i.e. CNRS-HEMTs [5, 6]. And, as the gain is 1 GΩ, the bandwidth is larger than 200 kHz. And, the equivalent input noise voltage PSD can be lower than 0.28 $(\text{nV})^2/\text{Hz}$ in $f > 10$ kHz, and the equivalent input noise current PSD is 0.62 $(\text{fA})^2/\text{Hz}$ at $f = 10$ kHz and 5.3 $(\text{fA})^2/\text{Hz}$ at $f = 100$ kHz. With the proposed TIA in CryoSTM, the STS measurements can be performed with the gain of 1 GΩ at the frequency of tens of kHz, and the STSNS measurements can be performed with the accuracy of 0.3 $(\text{fA})^2/\text{Hz}$ [1, 2]. However, these designed TIAs have not been fabricated and their performances have not been checked by measurements.

In this work, based on the proposed TIA design methods in Ref.[1], the TIA with the same circuit topology as that in Ref.[1] is designed and fabricated. A junction field effect transistor (JFET) is instead of the expensive CNRS-HEMT for the pre-amplifier. As a cheap demo, the performances of the JFET-based TIA, such as transimpedance gain, bandwidth, and inherent noises etc., are measured at 77 K. The measurement results are consistent with the calculation results and the simulation results in design. As an example, the realization of TIA in this work verifies the design method and analytical calculations for low-noise large-bandwidth high-gain TIA proposed in Ref.[1, 2]. As the gain of the JFET-based TIA is 1.13 GΩ, its bandwidth is about 97 kHz. And, its equivalent input noise voltage PSD is about 8 $(\text{nV})^2/\text{Hz}$ at $f = 10$ kHz and 3.7 $(\text{nV})^2/\text{Hz}$ at $f = 50$ kHz, and its equivalent input noise current PSD is about $26(\text{fA})^2/\text{Hz}$ at $f = 10$ kHz and 240 $(\text{fA})^2/\text{Hz}$ at $f = 50$ kHz. If this TIA is used for CryoSTM operating at 77 K, compared with FEMTO DE-DLPCA-200, the STS measurements with the same accuracy can be performed with 10 times higher speed, and the STSNS measurements can be performed at the frequency of tens of kHz.

2 Circuit of TIA and its amplifing performances

In CryoSTM, TIA is connected to a signal source circuit containing a tunnel junction (TJ) is denoted as TJ-TIA. The TJ-TIA circuit is shown in Fig.1, and the parameters of its components are shown in Table 1. Pre-amplifier (Pre-Amp) is shown in Fig.1(a1) and Fig.1(a2); Post-amplifier (Post-Amp) is shown in Fig.1(b); the feedback network with frequency compensation is shown in Fig.1(c); and the signal source circuit is shown in Fig.1(d). Cascading Pre-Amp and Post-Am form an inverting Amplifier (Inv-Amp). Connecting the feedback network on the Inv-Amp constitutes a TIA. TIA connected signal source circuit is TJ-TIA.

2.1 Pre-Amplifier

Fig.1(a1) annd (a2) show Pre-Amp. In Pre-Amp, the JFET is a N-Channel Depletion-Mode JFET, and SST4393-T1 as JFET is selected in this work [7]. SST4393-T1 can operate at 77K. The parameters of the components in the single-transistor amplifier circuit are shown in Table 1. $\overline{e_{\text{J}}^2}$ is the equivalent input noise voltage PSD and $\overline{i_{\text{J}}^2}$ is its equivalent input noise current PSD. The gate G of JFET is the input of Pre-Amp. O1 and O2 are

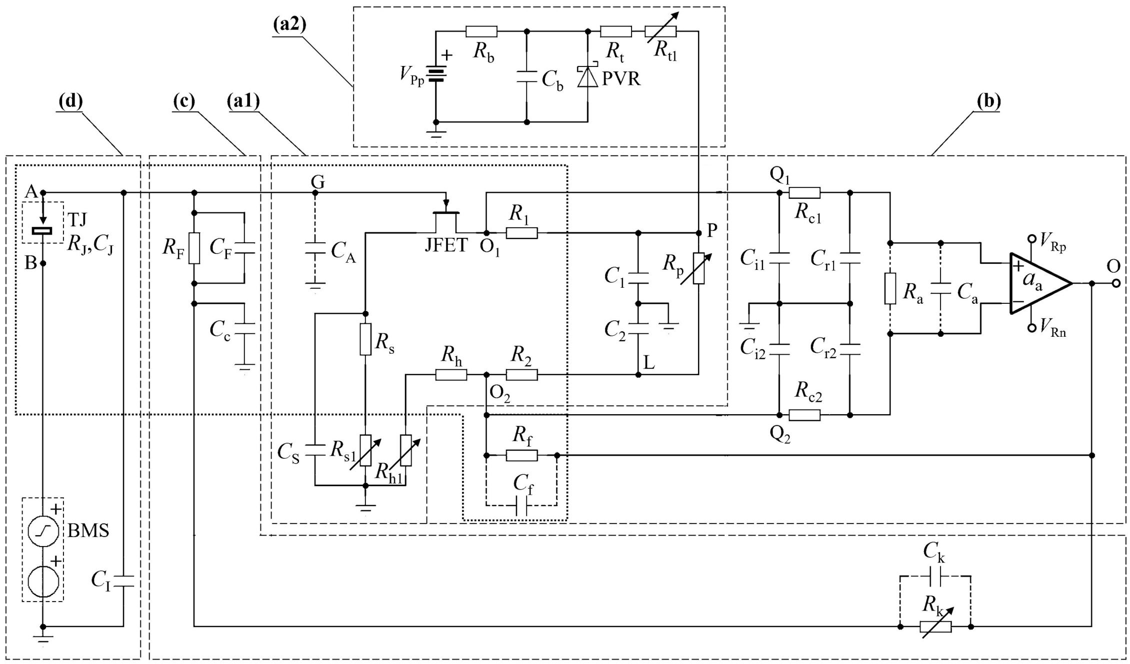

Figure 1: Circuit of the proposed TJ-TIA. Single HEMT amplifier part of Pre-Amp is shown in dashed box (a1), power supply of Pre-Amp in dashed box (a2), Post-Amp in dashed box (b), compensated feedback network in dashed box (c), and signal source circuit in dashed box (d). The components placed in the cryogenic zone are shown in the dotted box. The parameters of all components of TJ-TIA circuit are listed in Table 1.

called the inverting and positive outputs of Pre-Amp respectively, and they are connected to Post-Amp. JFET, R_{s}, R_{h}, R_1, and R_2 in Pre-Amp are placed in cryogenic zone at 77 K. And, $R_1 = R_2 = R_{\mathrm{L}}$. The capacitance of the cable connecting the tip of the CryoSTM to G is C_{I}. The JFET should be placed to the tip of the CryoSTM as close as possible, so that C_{I} is reduced to less than 0.5 pF. Variable resistors R_{s1}, R_{h1}, and R_{p} are placed at room temperature. $R_{\mathrm{H}} = R_{\mathrm{h}} + R_{\mathrm{h1}}$ and $R_{\mathrm{S}} = R_{\mathrm{s}} + R_{\mathrm{s}}$ are denoted. Fig.1(a2) shows the power supply for Pre-Amp, and the parameters of its components are shown in Table 1, where PVR is a precision voltage reference (LM4050-10 [8]). The output voltage of PVR is stable 10 V with typical error of ± 40 ppm. The noises from PVR are eliminated by C_1, C_2, and R_{T}. Here, $R_{\mathrm{T}} = R_{\mathrm{t}} + R_{\mathrm{t1}}$, and R_{t1} is a variable resistor. Keep R_{p} to 0, and adjust R_{s1}, R_{h1}, and R_{t1} to achieve JFET at the ideal operating point ($V_{\mathrm{ds}} = 1$ V, $I_{\mathrm{ds}} = 1$ mA) and the voltage at O1 equal to that at O2.

For Pre-Amp, adding AC voltage signal $\dot{V}$ on G, the output AC voltage difference between O1 and O2 is $\dot{V}_{\mathrm{pre}}$. The gain of Pre-Amp is $A_{\mathrm{vP}} = \dot{V}_{\mathrm{op}}/\dot{V}$. The upper limit cutoff frequency for Pre-Amp is larger than 5 MHz, since the transit frequency for JFET $g_{\mathrm{m}}/(2\pi C_{\mathrm{gs}})$ is larger than 200 MHz and the intrinsic gain for JFET $g_{\mathrm{m}}/g_{\mathrm{d}} < 30$. For Pre-Amp, A_{vP} can be obtained by the nodal analysis method [1]. In $f >> \max\{g_{\mathrm{m}}/(2\pi C_{\mathrm{S}}), 1/(2\pi R_{\mathrm{S}} C_{\mathrm{S}})\}$ (i.e. $f >> 12$ Hz) and $f \leq 1$ MHz, A_{vP} is

$$A_{\mathrm{vP}} \approx -g_{\mathrm{m}} R_{\mathrm{d}}, \tag{2.1}$$

Table 1: Parameters of all components of TJ-TIA

JFET SST4393-T1			
Gate–source resistance R_{A}			>10 TΩ
Transconductance g_{m}			8 mS
Channel conductance g_{d}			0.3 mS
Gate–source capacitance C_{gs}			9 pF
Gate–drain capacitance C_{gd}			5 pF
Drain–source voltage V_{ds}			1 V
Drain–source current I_{ds}			1 mA
Equivalent input noise voltge PSD $\overline{e_{\mathrm{J}}^2}$		10 kHz	7 $(\mathrm{nV})^2/\mathrm{Hz}$
		50 kHz	3 $(\mathrm{nV})^2/\mathrm{Hz}$
Equivalent input noise current PSD $\overline{i_{\mathrm{J}}^2}$		unkown	
Pre-Amp			
$R_{\mathrm{s}} + R_{\mathrm{s1}}$	520 ± 5 Ω	C_{S}	11 μF
$R_{\mathrm{h}} + R_{\mathrm{h1}}$	1520 ± 5 Ω	R_1, R_2	3.9 kΩ
R_{p}	5 ± 5 Ω		
C_1	22 μF	C_2	11 μF
PVR	LM4050-10	R_{b}	2 kΩ
$R_{\mathrm{t}} + R_{\mathrm{t1}}$	2280 ± 10 Ω	V_{Pp}	+15 V
THS4021 as Rear-OPA			
a_{a0}	94 dB	f_{b}	16 kHz
C_{a}	1.5 pF	R_{a}	1 MΩ
V_{Rp}	+5 V	V_{Rn}	-5 V
Equivalent input noise voltge PSD $\overline{e_{\mathrm{a}}^2}$		2.25 $(\mathrm{nV})^2/\mathrm{Hz}$ in $f > 10$ KHz	
Equivalent input noise current PSD $\overline{i_{\mathrm{a}}^2}$		4 $(\mathrm{pA})^2/\mathrm{Hz}$ in $f > 10$ KHz	
Post-Amp			
R_{f}	3.9 MΩ	C_{i1}, C_{i2}	160 pF
R_{c1},R_{c2}	100 Ω	C_{r1}, C_{r2}	50 pF
Feedback network			
R_{F}	1.13 GΩ	C_{F}	~ 3 pF
R_{k}	340 kΩ	C_{k}	~ 0.2 pF
C_{c}	10 nF		
Signal source circuit			
R_{J}	≥ 1 MΩ	C_{J}	~ 100 fF
C_{I}	~ 0.5 pF		

Note: $\pm$ indicates the variable resistance range. Without specification, the default value after $\pm$ is 0.

where $R_{\mathrm{d}} = R_{\mathrm{L}}/(1 + g_{\mathrm{d}}R_{\mathrm{L}})$. And, $A_{\mathrm{vP}} \approx -14.4$ (with the parameters in Table 1). The input capacitance of Pre-Amp is

$$C_{\mathrm{A}} = C_{\mathrm{gs}} + (1 - A_{\mathrm{vP}})C_{\mathrm{gd}}. \tag{2.2}$$

and $C_{\mathrm{A}} \approx 81$ pF (with the parameters in Table 1). The input resistance of Pre-Amp R_{A} is the gate-source resistance of JEFT. For SST4393-T1, $R_{\mathrm{A}} > 1$ TΩ, so R_{A} can be considered as infinity.

2.2 Post-Amplifier and Inverting-Amplifier

Fig.1(b) shows the Post-Amp circuit. An operational amplifier (OPA) is in the circuit, denoted as Rear-OPA. Rear-OPA used in this work is THS4021 [9]. R_{a} and C_{a} are the equivalent input resistance and capacitance of Rear-OPA, respectively. The positive input

of Rear-OPA is connected with a filter composed of R_{c1} and C_{r1}, which is connected to the inverting output of Pre-Amp O1 with Cable O1Q1. The inverting input of Rear-OPA is connected with a filter composed of R_{c2} and C_{r2}, which is connected to the positive output of Pre-Amp O2 with Cable O2Q2. $R_{c1} = R_{c2} = R_c$ and $C_{r1} = C_{r2} = C_r$. The ground capacitances of Cable O1Q1 and Cable O2Q2 are C_{i1} and C_{i2} respectively. The lengths of Cable O1Q1 and Cable O2Q2 are 1.6 m, and $C_{i1} = C_{i2} = C_i$ is about 160 pF. The feedback resistor R_f connects the output of Rear-OPA O and O2. C_f is the parasitic capacitance of R_f.

In Post-Amp, V_{Rp} is set at +5 V and $V_{Rn}$is set at -5 V, since the input voltage range of the oscilloscope (Rohde-Schwarz RTP) used in measurements is ±5 V. And, V_{Rp} (V_{Rn}) can be set at +15 V (-15 V) for the real application.

Cascade Pre-Amp and Post-Amp to form Inv-Amp. As JFET is at the ideal operating point with the grounded input G and the voltage at O1 is equal to that at O2, cascade Pre-Amp and Post-Amp, and then adjust R_p and R_{t1} to achieve JFET still at the ideal operating point ($V_{ds} = 1$ V, $I_{ds} = 1$ mA) and the voltage at the output of Inv-Amp O is 0. For the AC signal, the voltage gain of Inv-Amp $a_A(f)$ can be expressed as

$$a_A = A_{vP} A_{vR}. \tag{2.3}$$

a_A can be obtained with the nodal analysis method, and then A_{vR} can be obtained [1]. In $f >> \max\{g_m/(2\pi C_S), 1/(2\pi R_S C_S)\}$(i.e. $f >> 12$ Hz) and $f \leq 1$ MHz, A_{vR} is

$$A_{vR} \approx \frac{Z_f}{R_{HL}} \cdot \frac{1 + j2\pi f R_{HL} C_{ir}}{1 + j2\pi f R_d C_{ir}} \cdot \frac{1}{1 + \frac{Z_f}{a_a R_{HL}} + j2\pi f \frac{Z_f C_{ir}}{a_a}}, \tag{2.4}$$

where $Z_f = 1/(1/R_f + j2\pi f C_f)$, $R_{HL} = R_H R_L/(R_H + R_L)$, $C_{ir} = C_i + C_r$, and a_a is the voltage gain of the Rear-OPA. For THS4021, in $0 < f \leq 40$ MHz, $a_a \approx a_{a0}/(1 + jf/f_b)$, where $a_{a0} = 94$ dB, $f_b = 16$ kHz.

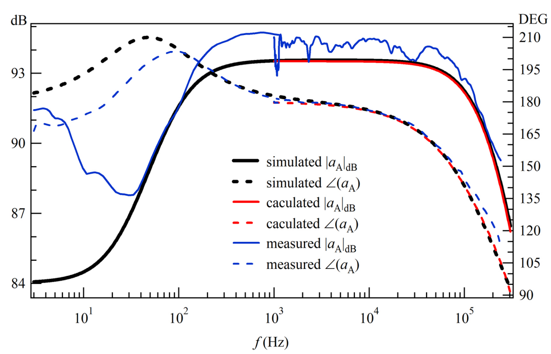

Figure 2: For the voltage gain of Inv-Amp $a_A(f)$, the simulated $|a_A(f)|_{dB}$ vs. f is the black solid curve and the simulated $\angle(a_A(f))$ vs. f is the black dashed curve. By Eqs.(2.1), (2.3), and (2.4), the calculated $|a_A(f)|_{dB}$ vs. f is the red solid curve and the calculated $\angle(a_A(f))$ vs. f is the red dashed curve. The measured $|a_A(f)|_{dB}$ vs. f is the blue solid curve and the measured $\angle(a_A(f))$ vs. f is the blue dashed curve.

With the parameters in Table 1, the performances of Inv-Amp are simulated with TINA-TI [10]. The simulated results of $a_A(f)$ are shown as the black curves in Fig.2.

The results of $a_{\mathrm{A}}(f)$ calculated by Eqs.(2.1), (2.3), and (2.4) are shown as the red curves in Fig..2, which are basically consistent with the simulated ones in 3 kHz$< f \leq 300$ kHz. $a_{\mathrm{A}}(f)$ is measured by a lock-in (Standford 865). In 100 Hz$< f < 240$ kHz, the measured results of $a_{\mathrm{A}}(f)$ are also basically consistent with those obtained by the TINA-TI simulations, as shown in Fig.2.

2.3 Frequency compensation of feedback loop

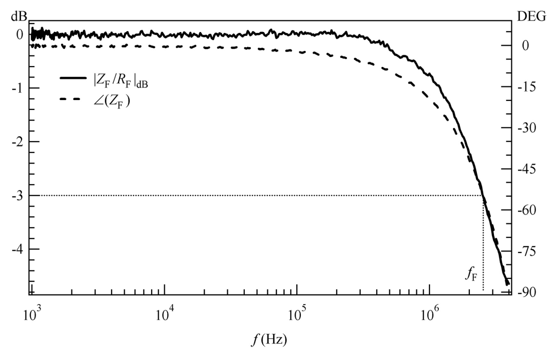

Figure 3: The measured $|Z_{\mathrm{F}}(f)/R_{\mathrm{F}}|_{\mathrm{dB}}$ (Solid curve) and the measured $\angle\left(Z_{\mathrm{F}}(f)\right)$ (Dashed curve). f_{F} is up to 2.25 MHz.

Fig.1(c) shows the feedback network in TIA. The frequency compensation method is described in Ref.[1]. The feedback impedance obtained by compensation is

$$Z_{\mathrm{F}}(f) \approx \frac{R_{\mathrm{k}}+R_{\mathrm{F}}}{1+j2\pi f R_{\mathrm{k}} C_{\mathrm{k}}} \approx \frac{R_{\mathrm{F}}}{1+j2\pi f R_{\mathrm{k}} C_{\mathrm{k}}},$$

$f_{\mathrm{F}} = 1/(2\pi f R_{\mathrm{k}} C_{\mathrm{k}})$ is the upper cut-off frequency of the feedback network. Here $R_{\mathrm{F}} = 1.13$ GΩ at 77 K. A small 2.7 pF capacitor is parallel to R_{F} with about 0.3 pF parasitic capacitance, therefore C_{F} as the total capacitance parallel to R_{F} is about 3 pF. $C_{\mathrm{c}} = 10$ nF, and $R_{\mathrm{k}} C_{\mathrm{c}} \sim R_{\mathrm{F}} C_{\mathrm{F}}$ as adjusting resistance $R_{\mathrm{k}} = 340$ kΩ. C_{k} is the parasitic capacitance of R_{k}. The measured results for $Z_{\mathrm{F}}(f)$ are shown in Fig.3, and f_{F} is up to 2.25 MHz. For the frequency compensated feedback network, it can be considered that Z_{F} is equal to R_{F} in $0 < f \leq 300$ kHz.

2.4 Transimpedance gain of TIA

Connect the feedback network with Inv-Amp to form TIA. Considering the TJ capacitance C_{J} ($C_{\mathrm{J}} \leq 100$ fF), the TJ impedance is $Z_{\mathrm{J}} = R_{\mathrm{J}}/(1+j2\pi f R_{\mathrm{J}} C_{\mathrm{J}})$. In $0 < f \leq 300$ kHz, for $R_{\mathrm{J}} \geq 1$ MΩ, the transimpedance gain of TIA A_{i} is [1]

$$A_{\mathrm{i}} \approx -\frac{R_{\mathrm{F}}}{1-\frac{1}{a_{\mathrm{A}}}-\frac{R_{\mathrm{F}}}{a_{\mathrm{A}} R_{\mathrm{A}}}-j2\pi f \frac{R_{\mathrm{F}} C_{\mathrm{A}}}{a_{\mathrm{A}}}},$$

Considering $R_{\mathrm{A}} >> R_{\mathrm{F}}$ and $|a_{\mathrm{A}}| >> 1$, A_{i} is

$$A_{\mathrm{i}} \approx -\frac{R_{\mathrm{F}}}{1-j2\pi f \frac{R_{\mathrm{F}} C_{\mathrm{A}}}{a_{\mathrm{A}}}}, \tag{2.5}$$

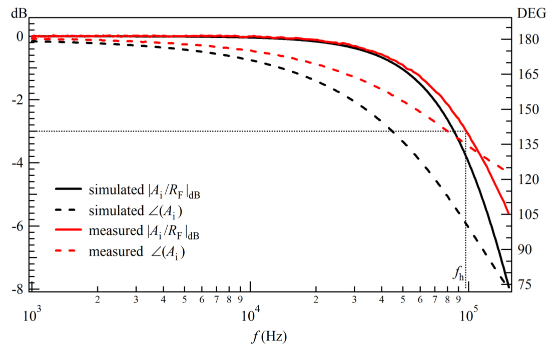

Figure 4: For the transimpedance gain of TIA A_i, the simulated $|A_i(f)/R_F|_{dB}$ (Black solid curve) and the simulated $\angle(A_i(f))$ (Black dashed curve), and the measured $|A_i(f)/R_F|_{dB}$ (Red solid curve) and the measured $\angle(A_i(f))$ (Red dashed curve). There is no "gain peaking" on the measuerd curve of $|A_i(f)/R_F|_{dB}$ vs. f, which is a evidence for the stability of TJ-TIA.

It is easily to verify that the caculated results of A_i by Eq.(2.5) are consistent with the simulated results with TINA-TI. In the TJ-TIA, the resistor of 3.9 MΩ is used as R_J instead of TJ between A and B. And, A_i with $R_J = 3.9$ MΩ (with parasitic capacitance $C_J \leq 100$ fF) is measured by a lock-in (Standford 865). Fig.4 shows the measured results and simulated results. The measured bandwidth of TIA f_h is about 97 kHz, while the simulated one is 86 kHz.

There is no "gain peaking" on the measuerd curve of $|A_i(f)/R_F|_{dB}$ vs. f with $R_J = 3.9$ MΩ (with $C_J \leq 100$ fF) in Fig.4, which is a evidence for the stability of TJ-TIA. In experiments, as the input of TIA is opened, i.e. $R_J = \infty$ ($C_J \sim 0$) and $C_I + C_A \approx C_A$ for TJ-TIA, measured by a oscilloscope (Rohde-Schwarz RTP), there is no self-oscillations found at the output of TIA. As the input of TIA is closed, i.e. $R_J = 0$ for TJ-TIA (TJ-TIA is degreed to Inv-Amp) there is no self-oscillations found at the output of TIA. Therefore, TJ-TIA is stable, and it can be work with enough accuracy as $R_J \geq 1$ MΩ.

3 Noise performences of TIA

For the circuit of TJ-TIA shown in Fig.1, we use the differential equivalent circuit with all noise sources to calculate its equivalent input noise. The details for the noise calculations are shown in Supplemental file [11]. In this work, the noise voltage PSD is measured by a vector analyzer (Agilent 89441A) or a oscilloscope (Rohde-Schwarz RTP).

3.1 Equivalent input noises of Inv-Amp

The equivalent input noise voltage and equivalent input noise current of JFET are denoted as e_J and i_J respectively. They may not independent. The equivalent input noise voltage and equivalent input noise current of the Rear-OPA are denoted as e_a and i_a respectively. They are commonly considered as independent.

The resistors R_s, R_1, R_2, and R_f are in the cryogenic zone of 77 K. And, their noises in $f > 1$ kHz are thermal noise, which can be neglected [1]. The resistor R_h is in the

cryogenic zone of 77 K. The resistor R_{h1} is in the room temperature zone, but it is very small. The noise voltage of R_{H} is e_{RH}. The noise voltage of the resistor R_{c1} is e_1, and that of R_{c2} is e_2. And, their noises in $f > 1$ kHz are thermal noise. These noise sources are independent. The equivalent input noise voltage and equivalent input noise current of Inv-Amp are denoted as e_{A} and i_{A} respectively. By the nodal analysis method and Wiener-Sinchin theorem, ignoring the minor terms, it is obtained that [11]

$$\overline{e_{\mathrm{A}}^2} \approx \overline{e_{\mathrm{J}}^2} + \left(\overline{e_{\mathrm{a}}^2} + \overline{e_1^2} + \overline{e_2^2}\right)/A_{\mathrm{vP}}^2, \tag{3.1}$$

$$\overline{i_{\mathrm{A}}^2} \approx \overline{i_{\mathrm{J}}^2} + (2\pi f)^2 \left[\frac{C_{\mathrm{A}}^2}{A_{\mathrm{vP}}^2}\left(\frac{R_{\mathrm{HL}}^2}{R_{\mathrm{H}}^2}\overline{e_{\mathrm{RH}}^2} + \overline{e_{\mathrm{a}}^2} + \overline{e_1^2} + \overline{e_2^2}\right) + \left(C_{\mathrm{gs}} + C_{\mathrm{gd}} + \frac{R_{\mathrm{HL}}}{R_{\mathrm{d}}}C_{\mathrm{A}}\right)^2 \frac{\overline{i_{\mathrm{a}}^2}}{g_{\mathrm{m}}^2}\right], \tag{3.2}$$

$$\begin{aligned}\overline{e_{\mathrm{A}} i_{\mathrm{A}}^*} = (\overline{i_{\mathrm{A}} e_{\mathrm{A}}^*})^* \approx \overline{e_{\mathrm{J}} i_{\mathrm{J}}^*} - j2\pi f \frac{C_{\mathrm{A}}}{A_{\mathrm{vP}}^2}\left(\frac{R_{\mathrm{HL}}^2}{R_{\mathrm{H}}^2}\overline{e_{\mathrm{RH}}^2} + \overline{e_{\mathrm{a}}^2} + \overline{e_1^2} + \overline{e_2^2}\right) \\ -j2\pi f\left(C_{\mathrm{gs}} + C_{\mathrm{gd}} + \frac{R_{\mathrm{HL}}}{R_{\mathrm{d}}}C_{\mathrm{A}}\right)\left(1 + \frac{R_{\mathrm{HL}}}{R_{\mathrm{d}}}\right)\frac{\overline{i_{\mathrm{a}}^2}}{g_{\mathrm{m}}^2},\end{aligned} \tag{3.3}$$

where $\overline{e_{\mathrm{A}}^2}$ is the equivalent input noise voltage PSD of Inv-Amp, $\overline{i_{\mathrm{A}}^2}$ is its equivalent input noise current PSD, $\overline{e_{\mathrm{A}} i_{\mathrm{A}}^*}$ is its equivalent input noise voltage-current PSD, and $\overline{i_{\mathrm{A}} e_{\mathrm{A}}^*}$ is its equivalent input noise current-voltage PSD.

It is difficult to obtain the equivalent input noise current PSD of JFET $\overline{i_{\mathrm{J}}^2}$ by measurements [6]. Let's assume that i_{J} is entirely generated by the channel noise current of JFET i_{c}, then $\overline{i_{\mathrm{J}}^2} \approx (2\pi f)^2 (C_{\mathrm{gs}} + C_{\mathrm{gd}})^2 \overline{i_{\mathrm{c}}^2}/g_{\mathrm{m}}^2$ [11]. It can be obtained that $\overline{e_{\mathrm{J}}^2} \approx \overline{i_{\mathrm{c}}^2}/g_{\mathrm{m}}^2$ [11]. Therefore,

$$\overline{i_{\mathrm{J}}^2} \approx (2\pi f)^2 (C_{\mathrm{gs}} + C_{\mathrm{gd}})^2 \overline{e_{\mathrm{J}}^2}. \tag{3.4}$$

By the same means,

$$\overline{e_{\mathrm{J}} i_{\mathrm{J}}^*} \approx -j2\pi f (C_{\mathrm{gs}} + C_{\mathrm{gd}}) \overline{e_{\mathrm{J}}^2}. \tag{3.5}$$

3.2 Equivalent input noises of TIA

For TIA, its equivalent input noise voltage and equivalent input noise current are denoted as e_{T} and i_{T} respectively. Based on Eqs..(3.1).(3.2).(3.3),(3.4), and .(3.5), the equivalent input noise voltage PSD of TIA $\overline{e_{\mathrm{T}}^2}$, its equivalent input noise current PSD $\overline{i_{\mathrm{T}}^2}$, its equivalent input noise voltage-current PSD $\overline{e_{\mathrm{A}} i_{\mathrm{A}}^*}$, and its equivalent input noise current-voltage PSD $\overline{i_{\mathrm{A}} e_{\mathrm{A}}^*}$ are [1, 11]

$$\overline{e_{\mathrm{T}}^2} \approx \overline{e_{\mathrm{J}}^2} + \left(\overline{e_{\mathrm{a}}^2} + \overline{e_1^2} + \overline{e_2^2}\right)/A_{\mathrm{vP}}^2, \tag{3.6}$$

$$\begin{aligned}\overline{i_{\mathrm{T}}^2} \approx \frac{4k_{\mathrm{B}}T}{R_{\mathrm{F}}} + (2\pi f)^2 (C_{\mathrm{gs}} + C_{\mathrm{gd}})^2 \overline{e_{\mathrm{J}}^2} + \frac{\overline{e_{\mathrm{J}}^2}}{R_{\mathrm{F}}^2} + \frac{\overline{e_{\mathrm{a}}^2} + \overline{e_1^2} + \overline{e_2^2}}{A_{\mathrm{vP}}^2 R_{\mathrm{F}}^2} \\ +(2\pi f)^2 \frac{C_{\mathrm{A}}^2}{A_{\mathrm{vP}}^2}\left(\frac{R_{\mathrm{HL}}^2}{R_{\mathrm{H}}^2}\overline{e_{\mathrm{RH}}^2} + \overline{e_{\mathrm{a}}^2} + \overline{e_1^2} + \overline{e_2^2}\right) + (2\pi f)^2 \left(C_{\mathrm{gs}} + C_{\mathrm{gd}} + \frac{R_{\mathrm{HL}}}{R_{\mathrm{d}}}C_{\mathrm{A}}\right)^2 \frac{\overline{i_{\mathrm{a}}^2}}{g_{\mathrm{m}}^2},\end{aligned} \tag{3.7}$$

$$\overline{e_{\rm T} i_{\rm T}^*} = (\overline{i_{\rm T} e_{\rm T}^*})^* \approx \frac{\overline{e_{\rm J}^2}}{R_{\rm F}} + \frac{\overline{e_{\rm a}^2} + \overline{e_1^2} + \overline{e_2^2}}{A_{\rm vP}^2 R_{\rm F}} - j2\pi f (C_{\rm gs} + C_{\rm gd}) \overline{e_{\rm J}^2}$$
$$-j2\pi f \frac{C_{\rm A}}{A_{\rm vP}^2} \left(\frac{R_{\rm HL}^2}{R_{\rm H}^2} \overline{e_{\rm RH}^2} + \overline{e_{\rm a}^2} + \overline{e_1^2} + \overline{e_2^2} \right)$$
$$-j2\pi f \left(C_{\rm gs} + C_{\rm gd} + \frac{R_{\rm HL}}{R_{\rm d}} C_{\rm A} \right) \left(1 + \frac{R_{\rm HL}}{R_{\rm d}} \right) \frac{\overline{i_{\rm a}^2}}{g_{\rm m}^2}, \tag{3.8}$$

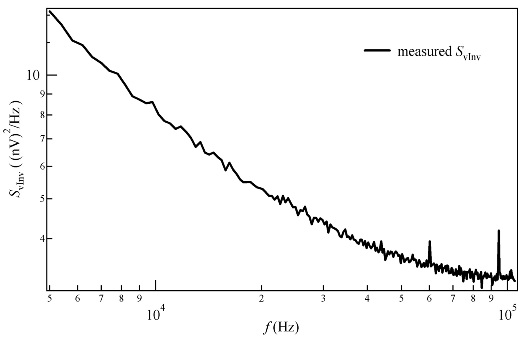

Figure 5: The measured equivalent input noise voltage PSD of TIA (i.e. the equivalent input noise voltage PSD of Inv-Amp) $S_{\rm vInv} = \overline{e_{\rm T}^2} = \overline{e_{\rm A}^2}$. It is about 8 (nV)^2/Hz at $f = 10$ kHz and 3.7 (nV)^2/Hz at $f = 50$ kHz.

As the input of TIA is grounded, the output noise voltage PSD of TIA (i.e. the output noise voltage PSD of Inv-Amp) $S_{\rm oInv}$ is measured. And, its equivalent input noise voltage PSD $S_{\rm vInv}$ (i.e. $\overline{e_{\rm T}^2}$) is obtained as $S_{\rm vInv} = S_{\rm oInv}/|a_{\rm A}|^2$. Fig.5 shows the curve for $S_{\rm vInv}$ vs. f. In Fig.5, $S_{\rm vInv} = \overline{e_{\rm T}^2}$ is about 8 (nV)^2/Hz at $f = 10$ kHz and 3.7 (nV)^2/Hz at $f = 50$ kHz, which are consistent with the values obained from Eq.(3.6) with the parameters in Table 1.

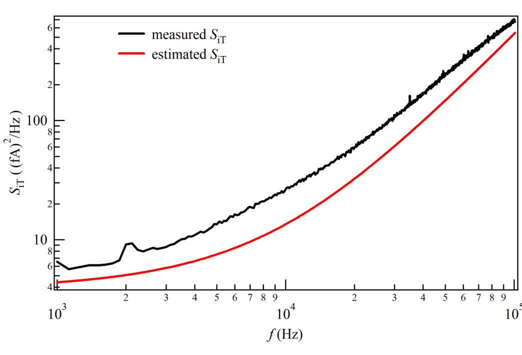

Figure 6: The measured equivalent input noise current PSD of TIA $S_{\rm iT} = \overline{i_{\rm T}^2}$. It is about 26 (fA)^2/Hz at $f = 10$ kHz and 240 (fA)^2/Hz at $f = 50$ kHz.

As the input of TIA is opened, the output noise voltage PSD of TIA $S_{\rm oT}(f)$ is measured, and the equivalent input noise current PSD of TIA $S_{\rm iT}$ (i.e. $\overline{i_{\rm T}^2}$) is obtained as $S_{\rm iT}(f) = S_{\rm oT}/|A_{\rm i}/|^2$. In Fig.6, the black curve is the measured $S_{\rm iT} = \overline{i_{\rm T}^2}$. The measured values are 26 (fA)^2/Hz at $f = 10$ kHz and 240 (fA)^2/Hz at $f = 50$ kHz.

$S_{\mathrm{iT}} = \overline{i_{\mathrm{T}}^2}$ is estimated by Eq.(3.7) with the parameters in Table 1, and the results are shown as the red curve in Fig6. The estimated values are 13.7(fA)^2/Hz at f = 10 kHz and 148(fA)^2/Hz at f = 50 kHz. The estimated valus of S_{iT} are slightly smaller than the measured ones, since we assume $\overline{i_{\mathrm{J}}^2}$ as the ideal minimum one.

In summary, for the TIA in this work, its equivalent input noise voltge PSD is about 8(nV)^2/Hz at f = 10 kHz and 3.7 (nV)^2/Hz at f = 50 kHz, and its equivalent input noise current PSD is 26 (fA)^2/Hz at f = 10 kHz and 240 (fA)^2/Hz at f = 50 kHz. Considering the bandwidth of TIA about 97 kHz and its gain of 1.13 GΩ, the TIA in this work has the lower noise and larger bandwidth comparing those of the present low-noise large-bandwidth high-gain TIAs [3, 12, 13].

4 Transimpedance gain of TIA obtained with noise measurements

In the TJ-TIA, the resistor of 3.9 MΩ is used as R_{J} instead of TJ between A and B, and B is grounded. S_{RJ} as the thermal noise current PSD of R_{J} is $S_{\mathrm{RJ}} = 4k_{\mathrm{B}}T/R_{\mathrm{J}} = 1090$ (fA)^2/Hz at $T = 77$ K. The output noise voltage of TJ-TIA $S_{\mathrm{oTJ}}(f)$ is measured in 500 Hz$< f \leq 100$ kHz. Obviously,

$$|A_{\mathrm{i}}|^2 = \frac{S_{\mathrm{oTJ}}(f) - S_{\mathrm{oT}}(f)}{S_{\mathrm{RJ}}}. \tag{4.1}$$

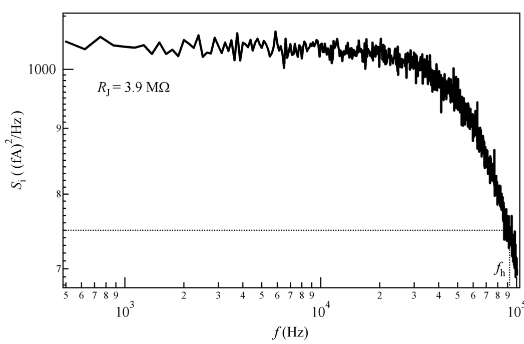

Figure 7: In the TJ-TIA, for a resistor R_{J} of 3.9 MΩ, the measured resullts for $S_{\mathrm{i}} = (S_{\mathrm{oTJ}} - S_{\mathrm{oT}})/R_{\mathrm{F}}^2$ in 500 Hz$< f \leq 100$ kHz. The measured bandwidth of TIA f_{h} is about 92 kHz.

Fig.7 shows the measured resullts for $S_{\mathrm{i}} = (S_{\mathrm{oTJ}} - S_{\mathrm{oT}})/R_{\mathrm{F}}^2$ in 500 Hz$< f \leq 100$ kHz. By Eq.(4.1), $S_{\mathrm{i}} = |A_{\mathrm{i}}(f)/R_{\mathrm{F}}|^2 S_{\mathrm{RJ}}$, so $|A_{\mathrm{i}}(f)/R_{\mathrm{F}}|$ can be charactered by S_{i}. At 1 kHz, $|A_{\mathrm{i}}/R_{\mathrm{F}}| \approx 1$ as shown in Fig.4, so S_{i}(1 kHz) in Fig.7 is about 1050 (fA)^2/Hz, aprroximate to $S_{\mathrm{RJ}} = 4k_{\mathrm{B}}T/R_{\mathrm{J}} = 1090$ (fA)^2/Hz. And, with this method, the measured bandwidth of TIA f_{h} is about 92 kHz, which is approximate to the value of 97 kHz measured by the lock-in in Section 2.4.

5 Conclusion

In Ref.[1, 2, 4], the designs of low-noise large-bandwidth high-gain transresistance amplifier (TIA) for Cryogenic STM are proposed. For them, Pre-Amp is made of CNRS-HEMTs. However, these designed TIAs have not been fabricated. In this work, for the proposed TIA in Ref.[1], we replace the expensive CHRS-HEMT with a junction field-effect transistor (JFET) SST4393-T1 that can operate at 77K. Based on the same design ideas, methods, and calculations, we design, fabricate, and measure the JFET-based TIA with the same circuit topology as that in Ref.[1]. The measured performances of the JFET-based TIA are in agreement with the simulated and calculated results, therefore the design methods and analytical calculations for low-noise large-bandwidth high-gain TIAs proposed in Ref.[1, 2] are verified. The transimpedance gain of the JFET-based TIA is 1.13 GΩ and its bandwidth is 97 kHz. its equivalent input noise voltage PSD is about 8 $(\mathrm{nV})^2/\mathrm{Hz}$ at 10k Hz and 3.7 $(\mathrm{nV})^2/\mathrm{Hz}$ at 50kHz, and its equivalent input noise current PSD is about 26 $(\mathrm{fA})^2/\mathrm{Hz}$ at 10 kHz and 240 $(\mathrm{fA})^2/\mathrm{Hz}$ at 50 kHz. If this TIA is used for CryoSTM operating at 77 K, the STS measurements and STSNS measurements can be performed at the frequency of tens of kHz.

Acknowledgment

This work is supported by Open Research Fund Program of the State Key Laboratory of Low-Dimensional Quantum Physics (Grant No. KF202212), Tsinghua University Initiative Scientific Research Program, National Natural Science Foundation of China (92065206), and the Innovation Program for Quantum Science and Technology (2021ZD0302400).

Declaration of competing interest

The author declares that they have no known competing financial interests or personal relationships that could have appeared to influence the work reported in this paper.

References

[1] Y.X. Liang, Ultra-low-noise transimpedance amplifier with a single HEMT in pre-amplifier for measuring shot noise in cryogenic STM, revised back to Ultramicroscopy, https://chinaxiv.org/abs/202212.00178?locale=en.

[2] Y.X. Liang, Low-noise large-bandwidth tansimpedance amplifier for measuring scanning tunneling shot noise spectra in cryogenic STM and its applications, Ultramicroscopy 234 (2022) 13466, https://doi.org/10.1016/j.ultramic.2022.113466.

[3] Data sheet of FEMTO DE-DLPCA-200 variable gain low noise current amplifier, https://www.femto.de/images/pdfdokumente/de-dlpca-200.pdf.

[4] Y.X. Liang, Ultra-low-noise transimpedance amplifier in cryogenic STM for studying novel quantum states by measuring shot noise, Low Temp. Phys 49 (2023) 676, https://doi.org/10.1063/10.0017824.

[5] Y.X. Liang, Q. Dong, M.C. Cheng, U. Gennser, A. Cavanna, and Y. Jin, Insight into low frequency noise induced by gate leakage current in AlGaAsGaAs high electron mobility transistors at 4.2 K, Appl. Phys. Lett. 99 (2011) 113505, https://doi.org/10.1063/1.3637054.

[6] Y. Jin, Q. Dong, A. Cavanna, U. Gennser, L. Couraud, and C. Ulysse, Ultra-low noise HEMTs for deep cryogenic low-frequency and highimpedance readout electronics, 12th IEEE International Conference on Solid-State and Integrated Circuit Technology (ICSICT) (2014).

[7] Data sheet of SST4393, https://www.alldatasheet.com/datasheet-pdf/pdf/600354/VISHAY/SST4393.html.

[8] Webpage of LM4050-10, https://www.ti.com/product/LM4050-N.

[9] Webpage of THS4021 OPA, https://www.ti.com/product/THS4021.

[10] TINA-TI is SPICE-based analog simulation program produced by Texas Instruments Inc., https://www.ti.com/tool/TINA-TI.

[11] Supplemental file.

[12] M. Stubian, J. Bobek, M. Setvin, U. Diebold, and M. Schmid, Fast low-noise ransimpedance amplifier for scanning tunneling microscopy and beyond, Rev. Sci. Instrum. 91, (2020). 074701.

[13] For AD8615, the typical value of its equivalent input noise voltage PSD is 40 $(\mathrm{nV})^2/\mathrm{Hz}$ in $f > 10$ kHz, and the typical value of its equivalent input noise current PSD is 2500 $(\mathrm{fA})^2/\mathrm{Hz}$ at $f = 1$ kHz. And, its equivalent input noise current PSD should be increased with the increase of frequency. For TIA with AD8615 as Pre-Amplifier in Macro-OPA [12], its equivalent input noise voltage (current) PSD cannot be lower than that of AD8615. Data sheet of AD8615, https://www.analog.com/media/en/technical-documentation/data-sheets/AD8615_8616_8618.pdf.

Supplemental file: Noise of the proposed TJ-TIA

S1 Noises of TIA

S1.1 The equivalent input noise voltage and equivalent input noise current of Inv-Amp

In Inv-Amp, the equivalent input noise voltage and equivalent input noise current of JFET are denoted as e_J and i_J respectively, and their harmonic components of f are denoted as E_J and I_J respectively. They may be not independent. g_m is the transconductance of JFET and g_d is channel conductance of JFET. A_{vP} is the gain of Pre-Amp. C_{gs} is the source-gate capacitance of JFET, C_{gd} is the drain-gate capacitance of JFET, $C_A = C_{gs} + (1- A_{vP})\, C_{gd}$ is the input capacitance of Pre-Amp, and C_{sd} is denoted as $C_{sd} = C_{gs} + C_{gd}$. The noise voltage of the resistors R_H is denoted as e_{RH}, and the harmonic components of f are denoted as E_{RH}. The noise voltage of the resistors R_1, R_2, and the feedback resistance R_f are denoted as e_{L1}, e_{L2} and e_f respectively, and the harmonic components of f are denoted as E_{L1}, E_{L2}, and E_f respectively. The noise voltage of the resistors R_{c1} and R_{c2} are denoted as e_1 and e_2 respectively, and the harmonic components of f are denoted as E_1 and E_2 respectively. Here, $R_1= R_2= R_L$ and $R_{c1} =R_{c2}= R_c$. All noises of R_H, R_1, R_2, R_{c1}, R_{c2}, and R_f above 1 kHz are thermal noise. $R_d = R_L//(1/g_d)$ and $R_{HL} = R_H//R_L$ are denoted. The equivalent input noise voltage and equivalent input noise current of Rear-OPA are denoted as e_a and i_a respectively, and the harmonic components of f are denoted as E_a and I_a respectively. These noise sources are independent of each other. For Inv-Amp consist of the Pre-Amp and Post-Amp, its equivalent input noise voltage and equivalent input noise current are e_A and i_A, the corresponding harmonic components of f are E_A and I_A respectively. With the same procedures mentioned in Supplemental file 4 of Ref.[SR1],

$$
\begin{aligned}
\begin{pmatrix} E_A \\ I_A \end{pmatrix} &= \begin{pmatrix} 0 \\ 1 \end{pmatrix} I_J + \begin{pmatrix} 1 \\ 0 \end{pmatrix} E_J - \begin{pmatrix} 1 \\ j(2\pi f)C_A \end{pmatrix} \frac{R_{HL}E_{RH}}{A_{vP}R_H} - \begin{pmatrix} 1 \\ j(2\pi f)C_{sd} \end{pmatrix} \frac{E_{L1}}{g_m R_L} - \begin{pmatrix} 1 \\ j(2\pi f)C_A \end{pmatrix} \frac{R_{HL}E_{L2}}{A_{vP}R_L} \\
&\quad - \begin{pmatrix} 1 \\ j(2\pi f)C_A \end{pmatrix} \frac{R_{HL}E_f}{A_{vP}R_f} - \begin{pmatrix} 1 \\ j(2\pi f)C_A \end{pmatrix} \frac{E_1 - E_2 - E_a}{A_{vP}} - \begin{pmatrix} 1 + R_{HL}/R_d \\ j(2\pi f)(C_{sd} + C_A R_{HL}/R_d) \end{pmatrix} \frac{I_a}{g_m}
\end{aligned}
$$
.

By Wiener-Khintchine theorem, ignoring the small quantities, such as the thermal

noise of R_1, R_2, and R_f,

$$\overline{e_A^2} \doteq \overline{e_J^2} + \left[\left(R_{HL}^2/R_H^2\right)\overline{e_{RH}^2} + \left(\overline{e_a^2}+\overline{e_1^2}+\overline{e_2^2}\right)\right]\Big/A_{vP}^2 + \left(1+R_{HL}/R_d\right)^2 \overline{i_a^2}\Big/g_m^2 \quad , \tag{s1}$$

$$\overline{i_A^2} \doteq \overline{i_J^2} + (2\pi f)^2\left[C_A^2\frac{R_{HL}^2}{R_H^2}\frac{\overline{e_{RH}^2}}{A_{vP}^2} + C_A^2\frac{\left(\overline{e_a^2}+\overline{e_1^2}+\overline{e_2^2}\right)}{A_{vP}^2} + \left(C_{sd}+\frac{R_{HL}}{R_d}C_A\right)^2\frac{\overline{i_a^2}}{g_m^2}\right], \tag{s2}$$

$$\begin{aligned}\overline{e_A i_A^*} = \left(\overline{i_A e_A^*}\right)^* \doteq \overline{e_J i_J^*} - j2\pi f C_A\left(\frac{R_{HL}^2}{R_H^2}\frac{\overline{e_{RH}^2}}{A_{vP}^2} + \frac{\overline{e_a^2}+\overline{e_1^2}+\overline{e_2^2}}{A_{vP}^2}\right)\\ - j2\pi f\left(C_{sd}+\frac{R_{HL}}{R_d}C_A\right)\left(1+\frac{R_{HL}}{R_d}\right)\frac{\overline{i_a^2}}{g_m^2}\end{aligned} . \tag{s3}$$

Here, $\overline{e_J^2}$ is the equivalent input noise voltage PSD of the JFET and $\overline{i_J^2}$ is their equivalent input noise current PSD. $\overline{e_a^2}$ is the equivalent input noise voltage PSD of the Rear-OPA and $\overline{i_a^2}$ is its equivalent input noise current PSD. $\overline{e_1^2}$, $\overline{e_2^2}$, and $\overline{e_{RH}^2}$ are the thermal noise voltage PSD of R_{c1}, R_{c2} and R_{RH} respectively.

$\overline{e_1^2} = \overline{e_2^2} = 4k_B T_R R_c = 1.66\ (\mathrm{nV})^2/\mathrm{Hz}$, where T_R is 300 K. $\overline{e_a^2} = 2.25\ (\mathrm{nV})^2/\mathrm{Hz}$ and $\overline{i_a^2} = 4\ (\mathrm{pA})^2/\mathrm{Hz}$ in $f \geq 10$ kHz [SR2]. In Eq.(s1), $\left(1+R_{HL}/R_d\right)^2\overline{i_a^2}\big/g_m^2$ is one order of magnitude smaller than $\overline{e_J^2}$. Further ignoring the small quantities in Eq.(s1),

$$\overline{e_A^2} \doteq \overline{e_J^2} + \left(\overline{e_a^2}+\overline{e_1^2}+\overline{e_2^2}\right)\Big/A_{vP}^2 \ , \tag{s4}$$

S1.1.1 *The equivalent input noise voltage and equivalent input noise current of JFET*

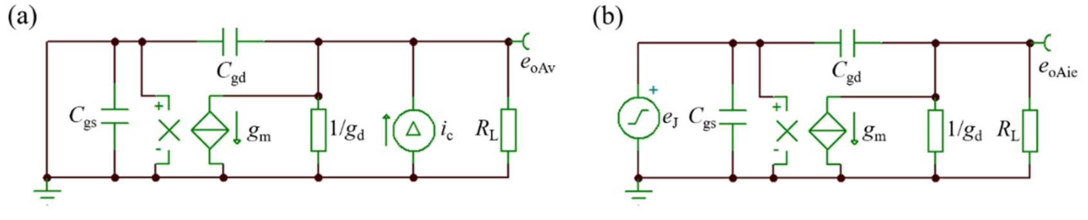

Figure s1 (a) JFET equivalent differential circuit with the input short-circuit with the channel noise current of JFET i_c, and the output noise voltage of e_{oAv}; (b) Noiseless JFET circuit with the equivalent input noise voltage of JFET e_J as the input signal, and the output noise voltage of e_{oAve}; the equivalency of the above two circuits means $e_{oAv} = e_{oAve}$.

In Eq.(s2) $\overline{i_J^2}$ is a major component, but it is very difficult to obtain its value by

measurements [SR3]. $\overline{i_J^2}$ is produced by many noise sources, and the JFET channel noise current i_c is one of them. The thermal noise of R_L can be ignored, and i_c is assumed as the only noise source. The equivalent differential circuit of the JFET with i_c with the input short-circuit is shown as Fig.s1(a), and the output noise is e_{oAv}. The noiseless circuit with the equivalent input noise voltage of the JFET e_J as the input signal is shown as Fig.s1(b), and the output noise is e_{oAve}. For calculating the equivalent input noise voltage of the JFET, the equations are established on $e_{oAv} = e_{oAve}$. Therefore, $\overline{e_J^2} \doteq \overline{i_c^2} / g_m^2$ can be obtained.

Assuming i_J is only caused by the JFET channel noise i_c, let us estimate its value. The JFET is at the same operating point for the input open-circuit and the input short-circuit, therefore the JFET channel noise is same. The equivalent differential circuit of the JFET with i_c with the input open-circuit is shown as Fig.s2(a), and the output noise is e_{oAi}. The noiseless circuit with the equivalent input noise current of the JFET i_J as the input signal is shown as Fig.s2(b), and the output noise is e_{oAie}. For calculating the equivalent input noise current of the JFET, the equations are established on $e_{oAi} = e_{oAie}$. Solving $e_{oAi} = e_{oAie}$, $\overline{i_J^2} \doteq (2\pi f)^2 C_{sd}^2 \overline{i_c^2} / g_m^2$. With $e_{oAi} = e_{oAie}$ and $e_{oAv} = e_{oAve}$, $\overline{e_J i_J^*} \doteq -j2\pi f C_{sd} \overline{i_c^2} / g_m^2$. Therefore,

$$\overline{i_J^2} \doteq (2\pi f)^2 C_{sd}^2 \overline{e_J^2}, \tag{s5}$$

$$\overline{e_J i_J^*} \doteq -j2\pi f C_{sd} \overline{e_J^2}. \tag{s6}$$

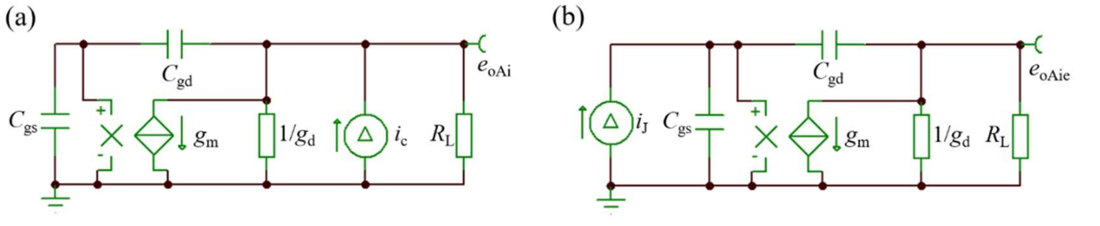

Figure s3.2 (a) JFET equivalent differential circuit with the input open-circuit with the channel noise current of JFET i_c, and the output noise voltage of e_{oAi}; (b) Noiseless JFET circuit with the equivalent input noise current of JFET i_J as the input signal, and the output noise voltage of e_{oAie}; the equivalency of the above two circuits means $e_{oAi} = e_{oAie}$.

***S1.1.2** The equivalent input noise current PSD and equivalent input noise voltage-current PSD of Inv-Amp*

Putting Eq.(s5) into Eq.(s2) and putting Eq.(s6) into Eq.(s3),

$$\overline{i_{\mathrm{A}}^2} \doteq (2\pi f)^2 \left[C_{\mathrm{sd}}^2 \overline{e_{\mathrm{J}}^2} + C_{\mathrm{A}}^2 \frac{R_{\mathrm{HL}}^2}{R_{\mathrm{H}}^2} \frac{\overline{e_{\mathrm{RH}}^2}}{A_{\mathrm{vP}}^2} + C_{\mathrm{A}}^2 \frac{\left(\overline{e_{\mathrm{a}}^2} + \overline{e_1^2} + \overline{e_2^2}\right)}{A_{\mathrm{vP}}^2} + \left(C_{\mathrm{sd}} + \frac{R_{\mathrm{HL}}}{R_{\mathrm{d}}} C_{\mathrm{A}} \right)^2 \frac{\overline{i_{\mathrm{a}}^2}}{g_{\mathrm{m}}^2} \right], \tag{s7}$$

$$\begin{aligned} \overline{e_{\mathrm{A}} i_{\mathrm{A}}^*} = \left(\overline{i_{\mathrm{A}} e_{\mathrm{A}}^*}\right)^* &\doteq -j2\pi f C_{\mathrm{sd}} \overline{e_{\mathrm{J}}^2} - j2\pi f C_{\mathrm{A}} \left(\frac{R_{\mathrm{HL}}^2}{R_{\mathrm{H}}^2} \frac{\overline{e_{\mathrm{RH}}^2}}{A_{\mathrm{vP}}^2} + \frac{\overline{e_{\mathrm{a}}^2} + \overline{e_1^2} + \overline{e_2^2}}{A_{\mathrm{vP}}^2} \right) \\ &- j2\pi f \left(C_{\mathrm{sd}} + \frac{R_{\mathrm{HL}}}{R_{\mathrm{d}}} C_{\mathrm{A}} \right) \left(1 + \frac{R_{\mathrm{HL}}}{R_{\mathrm{d}}} \right) \frac{\overline{i_{\mathrm{a}}^2}}{g_{\mathrm{m}}^2} \end{aligned}. \tag{s8}$$

S1.2 The equivalent input noise voltage and equivalent input noise current of TIA

The equivalent input noise voltage PSD of the TIA is denoted as $\overline{e_{\mathrm{T}}^2}$, its equivalent input noise current PSD is denoted as $\overline{i_{\mathrm{T}}^2}$, its equivalent input noise voltage-current PSD as $\overline{e_{\mathrm{T}} i_{\mathrm{T}}^*}$, and its equivalent input noise current-voltage PSD as $\overline{i_{\mathrm{T}} e_{\mathrm{T}}^*}$. With the same procedures mentioned in Supplemental file 4 of Ref.[SR1], It can be obtained that

$$\overline{e_{\mathrm{T}}^2} = \overline{e_{\mathrm{A}}^2}, \tag{s9}$$

$$\overline{i_{\mathrm{T}}^2} = \overline{i_{\mathrm{A}}^2} + 4k_{\mathrm{B}}T/R_{\mathrm{F}} + \overline{e_{\mathrm{A}}^2}/R_{\mathrm{F}}^2, \tag{s10}$$

$$\overline{e_{\mathrm{T}} i_{\mathrm{T}}^*} = \left(\overline{i_{\mathrm{T}} e_{\mathrm{T}}^*}\right)^* \doteq \overline{e_{\mathrm{A}} i_{\mathrm{A}}^*} + \overline{e_{\mathrm{A}}^2}/R_{\mathrm{F}}. \tag{s11}$$

Putting Eq.(s4) into Eq.(s9), putting Eqs. (s4) and (s7) into Eq.(s10), and putting Eqs. (s4) and (s8) into Eq.(s11),

$$\overline{e_{\mathrm{T}}^2} \doteq \overline{e_{\mathrm{J}}^2} + \left(\overline{e_{\mathrm{a}}^2} + \overline{e_1^2} + \overline{e_2^2}\right)/A_{\mathrm{vP}}^2, \tag{s15}$$

$$\begin{aligned} \overline{i_{\mathrm{T}}^2} &\doteq (2\pi f)^2 \left[C_{\mathrm{sd}}^2 \overline{e_{\mathrm{J}}^2} + C_{\mathrm{A}}^2 \frac{R_{\mathrm{HL}}^2}{R_{\mathrm{H}}^2} \frac{\overline{e_{\mathrm{RH}}^2}}{A_{\mathrm{vP}}^2} + C_{\mathrm{A}}^2 \frac{\left(\overline{e_{\mathrm{a}}^2} + \overline{e_1^2} + \overline{e_2^2}\right)}{A_{\mathrm{vP}}^2} + \left(C_{\mathrm{sd}} + \frac{R_{\mathrm{HL}}}{R_{\mathrm{d}}} C_{\mathrm{A}} \right)^2 \frac{\overline{i_{\mathrm{a}}^2}}{g_{\mathrm{m}}^2} \right], \\ &+ 4k_{\mathrm{B}}T/R_{\mathrm{F}} + 1/R_{\mathrm{F}}^2 \left[\overline{e_{\mathrm{J}}^2} + \left(\overline{e_{\mathrm{a}}^2} + \overline{e_1^2} + \overline{e_2^2}\right)/A_{\mathrm{vP}}^2 \right] \end{aligned} \tag{s16}$$

$$\overline{e_{\mathrm{T}}i_{\mathrm{T}}^{*}}=\left(\overline{i_{\mathrm{T}}e_{\mathrm{T}}^{*}}\right)^{*}\doteq\overline{e_{\mathrm{J}}^{2}}/R_{\mathrm{F}}+\left(\overline{e_{\mathrm{a}}^{2}}+\overline{e_{1}^{2}}+\overline{e_{2}^{2}}\right)\Big/\left(A_{\mathrm{vP}}^{2}R_{\mathrm{F}}\right)-j2\pi fC_{\mathrm{sd}}\overline{e_{\mathrm{J}}^{2}}$$
$$-j2\pi fC_{\mathrm{A}}\left(\frac{R_{\mathrm{HL}}^{2}}{R_{\mathrm{H}}^{2}}\frac{\overline{e_{\mathrm{RH}}^{2}}}{A_{\mathrm{vP}}^{2}}+\frac{\overline{e_{\mathrm{a}}^{2}}+\overline{e_{1}^{2}}+\overline{e_{2}^{2}}}{A_{\mathrm{vP}}^{2}}\right)-j2\pi f\left(C_{\mathrm{sd}}+\frac{R_{\mathrm{HL}}}{R_{\mathrm{d}}}C_{\mathrm{A}}\right)\left(1+\frac{R_{\mathrm{HL}}}{R_{\mathrm{d}}}\right)\frac{\overline{i_{\mathrm{a}}^{2}}}{g_{\mathrm{m}}^{2}} \qquad \text{(s17)}$$

S2 The equivalent input noise current of TJ-TIA

The TIA is connected with the signal source circuit to form a TJ-TIA. The equivalent input noise current PSD of aTJ-TIA $\overline{i_{\mathrm{in}}^{2}}$ can be obtained [SR1] by

$$\overline{i_{\mathrm{in}}^{2}}=\overline{i_{\mathrm{T}}^{2}}+\left(1/R_{\mathrm{J}}^{2}+\left(2\pi f\right)^{2}C_{\mathrm{IJ}}^{2}\right)\overline{e_{\mathrm{T}}^{2}}+\left(1/R_{\mathrm{J}}+j2\pi fC_{\mathrm{IJ}}\right)\overline{e_{\mathrm{T}}i_{\mathrm{T}}^{*}}+\left(1/R_{\mathrm{J}}-j2\pi fC_{\mathrm{IJ}}\right)\overline{i_{\mathrm{T}}e_{\mathrm{T}}^{*}}\,. \qquad \text{(s18)}$$

Here, $C_{\mathrm{IJ}}=C_{\mathrm{I}}+C_{\mathrm{J}}$. Putting Eq.(s4), (s7), and (s8) into Eq.(s18), the equivalent input noise current PSD of the proposed TJ-TIA $\overline{i_{\mathrm{in}}^{2}}$ is

$$\overline{i_{\mathrm{in}}^{2}}=4k_{\mathrm{B}}T/R_{\mathrm{F}}+\left(1/R_{\mathrm{J}}+1/R_{\mathrm{F}}\right)^{2}\left[\overline{e_{\mathrm{J}}^{2}}+\left(\overline{e_{\mathrm{a}}^{2}}+\overline{e_{1}^{2}}+\overline{e_{2}^{2}}\right)\Big/A_{\mathrm{vP}}^{2}\right]$$
$$+\left(2\pi f\right)^{2}\left[C_{\mathrm{sdJ}}^{2}\overline{e_{\mathrm{J}}^{2}}+C^{2}\frac{\overline{e_{\mathrm{a}}^{2}}+\overline{e_{1}^{2}}+\overline{e_{2}^{2}}+R_{\mathrm{HL}}^{2}\overline{e_{\mathrm{RH}}^{2}}/R_{\mathrm{H}}^{2}}{A_{\mathrm{vP}}^{2}}+\left(C_{\mathrm{sdI}}+\frac{R_{\mathrm{HL}}}{R_{\mathrm{d}}}C\right)^{2}\frac{\overline{i_{\mathrm{a}}^{2}}}{g_{\mathrm{m}}^{2}}\right], \qquad \text{(s19)}$$

where $C=C_{\mathrm{A}}+C_{\mathrm{I}}+C_{\mathrm{J}}$ and $C_{\mathrm{sdI}}=C_{\mathrm{gs}}+C_{\mathrm{gd}}+C_{\mathrm{I}}+C_{\mathrm{J}}$. Eq.(s19) is Eq.(8) in Article.

[SR1] Y.X. Liang, Ultra-low-noise transimpedance amplifier with a single HEMT in pre-amplifier for measuring shot noise in cryogenic STM, revised back to Ultramicroscopy, https://chinaxiv.org/abs/202212.00178?locale=en.

[SR2] Data sheet of THS4021 OPA, https://www.ti.com/lit/ds/symlink/ths4021.pdf.3.

[SR3] D. Quan, Y.X. Liang, D. Ferry, A. Cavanna, U. Gennser, L. Couraud, and Y. Jin, Ultra-low noise high electron mobility transistors for high-impedance and low frequency deep cryogenic readout electronics, Appl. Phys. Lett., 105 (2014) 013504 .